

Shell-model descriptions of mass 16-19 nuclei with chiral two- and three-nucleon interactions

Huan Dong¹, T. T. S. Kuo¹ and J. W. Holt²

¹*Department of Physics,
State University New York at Stony Brook
Stony Brook, New York 11794 and*

²*Physik Department, Technische Universität München, D-85747 Garching, Germany*

(Dated: August 7, 2018)

Shell-model calculations for several mass 16-19 nuclei are performed using the N^3LO two-nucleon potential V_{2N} with and without the addition of an in-medium three-nucleon potential V_{3N}^{med} , which is a density-dependent effective two-nucleon potential recently derived from the leading-order chiral three-nucleon force V_{3N} by Holt, Kaiser, and Weise. We first calculate the V_{low-k} low-momentum interactions from V_{2N} and V_{3N}^{med} . The shell-model effective interactions for both the sd one-shell and $sdpf$ two-shell model spaces are then obtained from these low-momentum interactions using respectively the Lee-Suzuki and the recently developed Okamoto and Suzuki iteration methods. The effects of V_{3N}^{med} to the low-lying states of ^{18}O , ^{18}F , ^{19}O and ^{19}F are generally small and attractive, mainly lowering the ground-state energies of these nuclei and making them in better agreements with experiments than those calculated with V_{2N} alone. The excitation spectra of these nuclei are not significantly affected by V_{3N}^{med} . The low-lying spectra of these nuclei calculated with the sd and $sdpf$ model spaces are closely similar to each other. Our shell-model calculations for ^{16}O indicate that the V_{3N}^{med} interaction is important and desirable for the binding energy of this nucleus.

PACS numbers: 21.60.Cs, 21.30.-x, 21.10.-k

I. INTRODUCTION

The nuclear shell model has been very successful in microscopic descriptions of nuclear structure, and in this approach the shell-model effective interaction V_{eff} has played an important role and its determination has been extensively studied [1–4]. As discussed in these references, V_{eff} may be determined using either an empirical approach where it is required to reproduce selected experimental data or a microscopic one where V_{eff} is derived from realistic nucleon-nucleon interactions using many-body methods. The interactions used in such microscopic calculations have been mostly the two-nucleon (NN) interaction V_{2N} [3, 4]. Should V_{eff} have also contributions from the three-nucleon (NNN) force V_{3N} in addition to the two-nucleon one? In fact the need of V_{3N} in nuclear many-body problems has long been recognized. The use of V_{2N} alone has been inadequate in reproducing the empirical nuclear matter saturation properties (see e.g. [5, 6] and references quoted therein). The inclusion of V_{3N} has been of essential importance in describing the binding energies and low-lying spectra of light nuclei [7–9] and in explaining the long half-life of the $^{14}C \rightarrow ^{14}N$ β -decay [10, 11]. Otsuka *et al.* [12] have shown that the inclusion of V_{3N} plays a crucial role in describing the oxygen isotopes near the drip line.

In the present work, we shall calculate the shell-model effective interactions for the sd and $sdpf$ shells using the chiral N^3LO two-nucleon potential V_{2N} [13] with and without the inclusion of the in-medium NNN force V_{3N}^{med} , which is a density-dependent two-nucleon potential recently derived from the leading-order chiral NNN force V_{3N} by Holt, Kaiser and Weise [10, 11]. We shall apply

these effective interactions to shell-model calculations for nuclei ^{18}O , ^{18}F , ^{19}O and ^{19}F , to study the effects of V_{3N}^{med} in these nuclei. We shall first calculate the low-momentum V_{low-k} interactions [14–16] from V_{2N} and V_{3N}^{med} . Our shell model effective interactions V_{eff} will then be calculated from these V_{low-k} interactions using a folded-diagram formalism [3, 4, 17, 18]. In this formalism, V_{eff} is given as a folded-diagram expansion. For the degenerate sd case, this expansion can be summed up using the commonly employed Lee-Suzuki (LS) iteration method [19, 20]. For the non-degenerate $sdpf$ case we shall sum up the expansion using the extended Krenciglowa-Kuo iteration method recently developed by Okamoto, Suzuki, Kumagai and Fujii (EKKO) [21, 25]. The EKKO method is efficient for deriving the effective interactions of non-degenerate model spaces such as the $sdpf$ two-shell space, and it can also be conveniently applied to degenerate model spaces such as the sd one-shell one. [25]

As mentioned earlier, the in-medium NNN potential V_{3N}^{med} is dependent on the nuclear medium density ρ . We shall study this ρ dependence for both low and moderately high densities. Clearly, at zero density V_{3N}^{med} vanishes. Nuclear matter calculations using V_{2N} alone have not been able to satisfactorily reproduce the empirical nuclear matter saturation properties [5, 6]. It may be useful to study if the ρ dependence of V_{3N}^{med} near the nuclear matter saturation density ρ_0 (0.16 fm^{-3}) may play an important role for nuclear matter saturation. We shall do so by carrying out nuclear matter calculations with and without the inclusion of V_{3N}^{med} . Similarly this dependence may also be important for closed-shell nuclei, such as ^{16}O , whose nucleons are embedded in a nuclear

medium of densities near ρ_0 . We shall calculate closed-shell nucleus ^{16}O with and without the inclusion of V_{3N}^{med} , as a further study of its effect near ρ_0 . The valence nucleons, such as those of ^{18}O , are in a medium of densities much less than ρ_0 . Thus our shell-model calculations for valence nuclei mentioned earlier are a study of V_{3N}^{med} at low densities.

The organization of the present paper is as follows. We shall describe some details about the derivation of V_{3N}^{med} from V_{3N} in section II. It may be noted that V_{3N}^{med} is an effective density-dependent two-nucleon interaction, which is more convenient than its underlying three-nucleon potential for nuclear many-body calculations. The methods we shall employ for the derivation of the shell-model effective interactions V_{eff} from V_{2N} and V_{3N}^{med} will be outlined there. In section III we shall present first our results of nuclear matter calculations using V_{2N} with and without the inclusion of V_{3N}^{med} . The ring-diagram formalism [5, 6] employed for our nuclear matter calculations will also be outlined. Next we shall report the results of a similar ring-diagram calculation for ^{16}O . Results of our shell-model calculations of ^{18}O , ^{18}F , ^{19}O and ^{19}F using V_{2N} with and without the inclusion of V_{3N}^{med} will be presented and discussed in this section. A summary and conclusion is presented in section IV.

II. FORMALISM

We first describe how we include the effects of the leading-order chiral three-nucleon interaction, V_{3N} , in our calculations. We consider the nuclear interaction V as given by $V = (V_{2N} + V_{3N}^{med})$, where V_{2N} is the N³LO Idaho two-nucleon potential [13] and V_{3N}^{med} is a density-dependent two-body interaction obtained from the chiral three-nucleon force by closing one pair of external lines and summing over the filled Fermi sea of nucleons. The leading contribution to V_{3N} occurs at N²LO in the chiral power counting and is composed of a long-range two-pion exchange component $V_{3N}^{2\pi}$, a medium-range one-pion exchange term $V_{3N}^{1\pi}$, and a pure contact interaction V_{3N}^{ct} :

$$V_{3N}^{(2\pi)} = \sum_{i \neq j \neq k} \frac{g_A^2}{8f_\pi^4} \frac{\vec{\sigma}_i \cdot \vec{q}_i \vec{\sigma}_j \cdot \vec{q}_j}{(\vec{q}_i^2 + m_\pi^2)(\vec{q}_j^2 + m_\pi^2)} F_{ijk}^{\alpha\beta} \tau_i^\alpha \tau_j^\beta, \quad (1)$$

$$V_{3N}^{(1\pi)} = - \sum_{i \neq j \neq k} \frac{g_A c_D}{8f_\pi^4 \Lambda_\chi} \frac{\vec{\sigma}_j \cdot \vec{q}_j}{\vec{q}_j^2 + m_\pi^2} \vec{\sigma}_i \cdot \vec{q}_j \vec{\tau}_i \cdot \vec{\tau}_j, \quad (2)$$

$$V_{3N}^{(ct)} = \sum_{i \neq j \neq k} \frac{c_E}{2f_\pi^4 \Lambda_\chi} \vec{\tau}_i \cdot \vec{\tau}_j, \quad (3)$$

where $g_A = 1.29$, $f_\pi = 92.4\text{MeV}$, $\Lambda_\chi = 700\text{MeV}$, $m_\pi = 138.04\text{MeV}/c^2$ is the average pion mass, $\vec{q}_i = \vec{p}_i' - \vec{p}_i$ is the difference between the final and initial momentum of

nucleon i and

$$F_{ijk}^{\alpha\beta} = \delta^{\alpha\beta} (-4c_1 m_\pi^2 + 2c_3 \vec{q}_i \cdot \vec{q}_j) + c_4 \epsilon^{\alpha\beta\gamma} \tau_k^\gamma \vec{\sigma}_k \cdot (\vec{q}_i \times \vec{q}_j). \quad (4)$$

The low-energy constants $c_1 = -0.76\text{GeV}^{-1}$, $c_3 = -4.78\text{GeV}^{-1}$, and $c_4 = 3.96\text{GeV}^{-1}$ appear already in the N²LO two-nucleon potential and are therefore constrained by low-energy NN phase shifts [27]. The low-energy constants c_D and c_E are typically fit to reproduce the properties of light nuclei [7–9].

A general three-body force may be written in second quantization as

$$\hat{V}_{3N} = \frac{1}{36} \sum_{123456} V([123], [456]) b_1^\dagger b_2^\dagger b_3^\dagger b_6 b_5 b_4, \quad (5)$$

where the antisymmetrized matrix element is

$$V([123], [456]) \equiv \langle 123 | V_{3N} | 456 + 645 + 564 - 654 - 546 - 465 \rangle. \quad (6)$$

Here $\langle 123 | V_{3N} | 456 \rangle$ is a simple product matrix element, and b^\dagger and b are creation and destruction operators defined with respect to the particle-hole vacuum $|C\rangle$ with $b_k |C\rangle = 0$ for all k . From eqs. (1-4) we can write $V_{3N} = V_{3N}^{(1)} + V_{3N}^{(2)} + V_{3N}^{(3)}$, where $V_{3N}^{(i)}$ is the component of V_{3N} that is symmetric with respect to the interchange $j \leftrightarrow k$. Now we contract one pair of the b^\dagger and b operators of the above \hat{V}_{3N} (both operators must be holes), and this leads to an effective two-body force

$$\hat{V}_{3N}^{med} = \frac{1}{4} \sum_{1245} D([12], [45]) b_1^\dagger b_2^\dagger b_5 b_4, \quad (7)$$

with

$$D([12], [45]) = \sum_{i \leq k_F} \left[\langle i12 | V_{3N}^{(2)} | i45 \rangle + \langle 1i2 | V_{3N}^{(2)} | 4i5 \rangle + \langle 12i | V_{3N}^{(2)} | 45i \rangle - \langle 1i2 | V_{3N}^{(2)} | i45 \rangle - \langle i12 | V_{3N}^{(2)} | 4i5 \rangle - \langle 1i2 | V_{3N}^{(2)} | 4i5 \rangle - \langle 1i2 | V_{3N}^{(2)} | 45i \rangle + \langle i12 | V_{3N}^{(2)} | 45i \rangle + \langle 12i | V_{3N}^{(2)} | i45 \rangle - (4 \leftrightarrow 5) \right], \quad (8)$$

where $4 \leftrightarrow 5$ denotes the nine exchange terms. The above result is unchanged when $V_{3N}^{(2)}$ is replaced by either $V_{3N}^{(1)}$ or $V_{3N}^{(3)}$. In our calculations we consider a background medium of symmetric nuclear matter at constant density characterized by a Fermi momentum k_F . In this way analytic expressions can be obtained for V_{3N}^{med} , as shown in refs. [10, 11]. The above is a density dependent effective ‘two-nucleon’ interaction which, unlike its underlying three-nucleon force, can be readily used in many-body problems. As detailed in [11], the partial-wave potentials of the above V_{3N}^{med} have been derived from the lowest-order three-nucleon force. We shall use

them in our calculations, namely we shall consider the nucleon interaction as given by $(V_{2N} + V_{3N}^{med})$.

We use the folded-diagram theory [3, 4, 17, 18] to calculate the effective interaction. Briefly speaking, in this theory V_{eff} is given by a folded-diagram series

$$V_{eff} = \hat{Q} - \hat{Q}' \int \hat{Q} + \hat{Q}' \int \hat{Q} \int \hat{Q} - \hat{Q}' \int \hat{Q} \int \hat{Q} \int \hat{Q} \dots, \quad (9)$$

where \hat{Q} represents a so-called \hat{Q} -box consisted of irreducible diagrams, as illustrated by the 1st- and 2nd-order diagrams of Fig. 1. (The \hat{Q}' -box is the same as the \hat{Q} -box except that \hat{Q}' does not have diagrams 1st-order in the interaction.) Suppose we include only V_{2N} . Then each vertex in the diagrams shown represents a V_{low-k} low-momentum interaction [14–16] derived from V_{2N} . When we include also V_{3N}^{med} in the calculation of V_{eff} , the \hat{Q} -box diagrams for effective interactions will have a specific type of V_{3N}^{med} vertices as illustrated in Fig. 2. Recall that diagram d4 of Fig. 1 represents the interaction between two valence nucleons via V_{2N} . This diagram becomes diagram (a) of Fig. 2 if its V_{2N} is replaced by V_{3N}^{med} . Here the two valence nucleons have to have the participation of a sea-nucleon (below Fermi sea) in order to activate V_{3N} , as indicated by the hole-line loop in the diagram. (Note each V_{3N}^{med} vertex of Fig. 2 represents a V_{low-k} interaction derived from V_{3N}^{med} .) Similarly diagram d1 of Fig. 1 represents the interaction of a valence nucleon with a sea-nucleon via the two-nucleon interaction V_{2N} . If this interaction is replaced by V_{3N}^{med} , this diagram becomes diagram (b) of Fig. 2. V_{3N} must involve three nucleons, and hence here the valence nucleon interacts with ‘two’ sea-nucleons as indicated by the two hole-line loops attached to V_{3N} . Diagram (c) is the V_{3N} core polarization diagram corresponding to diagram d7 of Fig. 1. Again here one hole-line loop is needed for each vertex to activate V_{3N} . As seen from Eqs. (31) and (32), V_{3N}^{med} requires the involvement of at least one sea-nucleon, and it is this requirement which is reflected by the hole-line loops attached to the V_{3N} vertices in Fig. 2. To summarize, the \hat{Q} -box diagrams of Fig. 1 are used for calculating V_{eff} when we use only V_{2N} , while additional diagrams as illustrated by Fig. 2 are also included when the interaction is consisted of both V_{2N} and V_{3N} .

After obtaining the \hat{Q} -box, we calculate the effective interaction of Eq. (9) using iteration methods. The LS method [19, 20] is convenient for degenerate model spaces, and it is used to calculate the *sd* one-shell effective interactions. For the non-degenerate *sdpf* two-shell effective interactions, one can use either the Krenciglowa-Kuo iteration method (KK) [23, 24] or the recent extended KK method (EKKO) of Okamoto *et al.* [21]. Both the EKKO and KK methods are convenient for calculating the effective interaction for non-degenerate model spaces, while the EKKO method being more efficient (faster converging rate). [25]. The main difference between the EKKO and KK methods is the following.

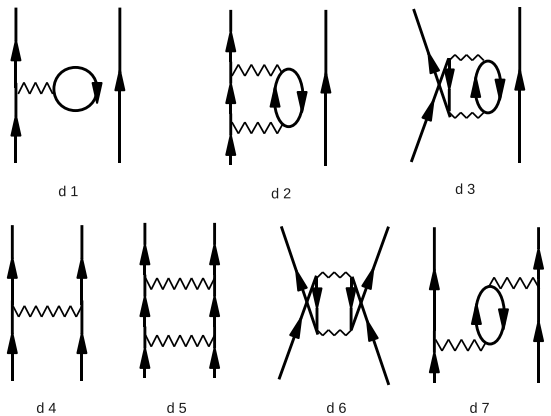


FIG. 1: Low-order diagrams constituting the \hat{Q} -box.

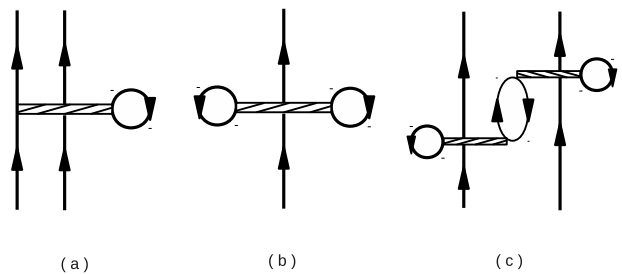


FIG. 2: \hat{Q} -box diagrams with three-nucleon forces. Each V_{3N}^{med} interaction is represented by a ‘narrow band with hole-line-loop’ vertex.

The KK method employs the irreducible vertex function \hat{Q} -box which may be written as

$$\hat{Q}(\omega) = [PVP + PVQ \frac{1}{\omega - QHQ} QVP]_L \quad (10)$$

where V represents the NN interaction, P denotes the model-space projection operator, and $Q \equiv (1 - P)$. The energy variable ω is determined self-consistently [19, 20]. Note that \hat{Q} contains only valence-linked diagrams as indicated by the subscript L . In the EKKO method, the above \hat{Q} -box is replaced by the \hat{Z} -box defined by [21, 25]

$$\hat{Z}(\omega) = \frac{1}{1 - \hat{Q}_1(\omega)} [\hat{Q}(\omega) - \hat{Q}_1(\omega)P(\omega - H_0)P], \quad (11)$$

where \hat{Q}_1 is the first derivative $d\hat{Q}/d\omega$. When the P- and Q-space are not sufficiently separated, the above \hat{Q} -box may have singularities. An important advantage of the EKKO method is that the \hat{Z} -box is well behaved even when the corresponding \hat{Q} -box is singular, overcoming the above singularity difficulty and making the EKKO method more efficient [21, 25]. We shall calculate the *sdpf* two-shell effective interactions using both the EKKO and KK iteration methods, to cross check their convergences.

III. RESULTS AND DISCUSSION

As described in section II, we shall calculate the shell-model effective interactions with the inclusion of the medium-dependent three-nucleon force V_{3N}^{med} which is obtained from a chiral NNN force by integrating one participating sea-nucleon over the Fermi sea. The V_{3N}^{med} interaction is a density dependent effective interaction, and we shall first carry out nuclear matter calculations with the inclusion of V_{3N}^{med} , to study the properties of this interaction at various densities near the nuclear matter saturation density ρ_0 . Before doing so, we need to choose or decide the low-energy constant of V_{3N} (see Eqs. (1-3)) to be used in our calculations. The low-energy constants c_1 , c_3 and c_4 of $V_{3N}^{(2\pi)}$ are well determined; they are constrained by low-energy NN scattering data [27]. Their values so determined (section II) will be used in the present work. But the low-energy constants c_D and c_E , of $V_{3N}^{(1\pi)}$ and $V_{3N}^{(ct)}$ respectively, are less well known; their values determined from properties of light nuclei exhibit considerable variations [7–10]. The V_{3N}^{med} interaction depends explicitly on the Fermi momentum k_F which is well defined for nuclear matter. But k_F is not well defined for finite nuclei, causing uncertainty in determining the low-energy constants of V_{3N}^{med} from properties of finite nuclei. But for nuclear matter, k_F is well defined; we have thus chosen to study these constants by way of nuclear matter calculations with V_{3N}^{med} included.

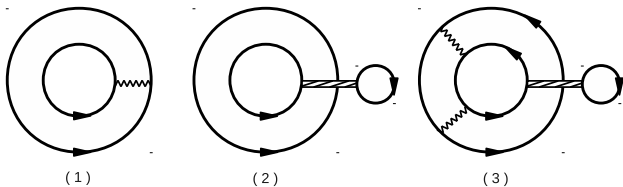


FIG. 3: Nuclear matter ring diagrams with vertices from V_{2N} (wavy line) and V_{3N}^{med} (narrow band with hole-line-loop).

We calculate the equation of state (EOS) for symmetric nuclear matter using a ring-diagram formalism [5, 6]. A brief description of this formalism is presented below, to outline how we include V_{3N}^{med} in our calculations. Using familiar renormalization procedures [14–16], we first calculate the low-momentum interactions $V_{low-k}^{2N}(\Lambda)$ and $V_{low-k}^{3N}(\Lambda)$ respectively from V_{2N} [13] and V_{3N}^{med} . A common decimation scale of $\Lambda = 2.1\text{fm}^{-1}$ is employed. This value is chosen because at this scale the low-momentum interactions derived from different NN potentials [13, 29–31] are remarkably close to each other [16], leading to a nearly unique low-momentum interaction. Using the above ring-diagram framework, the ground-state energy shift ΔE is given by the all-order sum of the $pphh$ ring diagrams as illustrated in Fig. 3. (ΔE_0 is defined as $(E_0 - E_0^{free})$ where E_0 is the true ground state energy and E_0^{free} that for the non-interacting system.) As shown

in Fig.3, diagram (1) is a 1st-order ring diagram with its vertex V_{2N}^{low-k} calculated from the $N^3\text{LO}$ chiral NN potential [13]. Similarly diagram (2) is a 1st-order ring diagram with V_{3N}^{low-k} obtained from the lowest order chiral V_{3N} as described in section II. Diagram (3) has vertices from both V_{2N}^{low-k} and V_{3N}^{low-k} . Similar to Fig. 2, to have the pair of nucleons in the ring diagrams interact with V_{3N} there must be the participation of a third nucleon. Thus the V_{3N} vertices in Fig. 3 all have a one-hole-line loop attached to them.

With these ring diagram summed to all orders, the ground-state energy shift for nuclear matter is given as

$$\Delta E_0 = \int_0^1 d\lambda \sum_m \sum_{ijkl < \Lambda} Y_m(ij, \lambda) Y_m^*(kl, \lambda) \times \langle ij | [V_{low-k}^{2N}(\Lambda) + V_{low-k}^{3N}(\Lambda)] | kl \rangle. \quad (12)$$

The transition amplitudes above are $Y_m^*(kl, \lambda) = \langle \Psi_m(\lambda, A-2) | \beta(kl) | \Psi_0(\lambda, A) \rangle$, where $\Psi_0(\lambda, A)$ denotes the true ground state of nuclear matter which has A particles, $\Psi_m(\lambda, A-2)$ the m th true eigenstate of the $(A-2)$ system, and $\beta(kl) = b_l b_k$ if $(k, l) > k_F$ and $= b_k^\dagger b_l^\dagger$ if $(k, l) \leq k_F$. Note that λ is a strength parameter, integrated from 0 to 1. The amplitudes Y are calculated from a RPA equation [5, 6, 26] based on the $(V_{2N} + V_{3N}^{med})$ interactions. Note that our calculation is the same as the usual Hartree-Fock (HF) one if we include only the 1st-order ring diagrams (1) and (2) of Fig. 4, and in this case the above Y amplitude becomes $Y(ij) = n_i n_j$ where $n_i = 1$ for $i < k_F$ and $= 0$ otherwise. Our ring-diagram calculations include particle-hole fluctuations of the Fermi sea, while not so for the HF calculations.

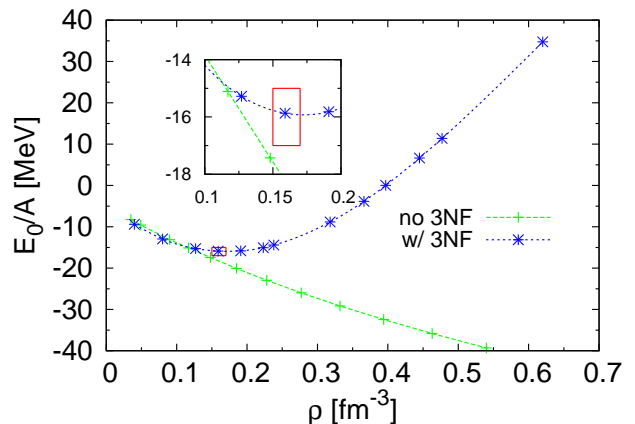


FIG. 4: Ring-diagram equation of state for symmetric nuclear matter calculated with (w/ 3NF) and without (no 3NF) V_{3N}^{med} .

We have carried out ring-diagram calculations for symmetric nuclear matter using a wide range of values for c_D and c_E . Our results with $c_D = -2.7$ and $c_E = 0.7$ are displayed in Fig. 4; they give $E_0/A \simeq -16\text{MeV}$ and $\rho_0 \simeq 0.16\text{fm}^{-3}$, both in satisfactory agreement with the empirical values. Two curves are shown in the figure,

one with V_{2N} alone and the other with the addition of V_{3N}^{med} . Comparing with the V_{2N} curve, it is of interest that the effect of V_{3N}^{med} is slightly attractive for low densities ($< \sim 2\rho_0/3$) while becomes strongly repulsive at high densities. Recall that we have used a common decimation scale of $\Lambda = 2.1\text{fm}^{-1}$ [16] for both V_{2N}^{low-k} and V_{3N}^{low-k} . It is of interest that in the ring-diagram calculations with Brown-Rho scaling [5, 6] a large Λ of $\sim 3.0\text{fm}^{-1}$ is needed for obtaining satisfactory nuclear matter saturation properties, while in the present calculation with V_{3N}^{med} satisfactory results can be obtained with the use of a smaller Λ (2.1fm^{-1}).

We have calculated the HF s.p. spectrum ϵ_k in nuclear matter with the inclusion of both V_{2N} and three-nucleon force V_{3N}^{med} . The inclusion of the latter has been found to have significant effect to the spectrum. ϵ_k can be well fitted by the quadratic expression $(k^2\hbar^2/(2m^*) + \Delta)$ where m^* is the effective mass and Δ is a well-depth parameter representing the s.p. energy at zero momentum. In Fig. 5 we present our results for Δ and m/m^* for various densities. Two curves are shown: the lower one without and the top one with the inclusion of V_{3N}^{med} . The densities for the 7 data points of each curve are, from left to right, $(0.25, 0.5, 1.0, 1.5, 2.0, 2.5, 3.0\rho_0)$ respectively. As shown by the lower curve of the figure, Δ and m/m^* both vary monotonically with the density when only V_{2N} is employed. With increasing density, Δ becomes increasingly more negative and m/m^* increasingly larger, exhibiting no saturation (up to $3.0\rho_0$). The trend is quite different for the upper curve where the three-nucleon force is included. Here m/m^* still monotonically increases with density, but Δ arises after saturation, approaching zero at some higher density. It is of interest that V_{3N}^{med} has a large effect in raising the chemical potential of nucleons in high density nuclear matter; this raise of the chemical potential may play an important role in enabling such nucleons decaying into other baryons such as hyperons.

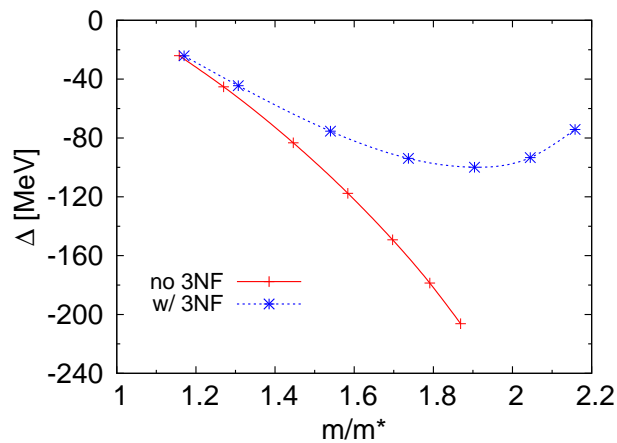


FIG. 5: Comparison of m^* and Δ for the in-medium s.p. spectrum calculated with (w/ 3NF) and without (no 3NF) V_{3N}^{med} . See text for other explanations.

As indicated by Fig. 4, our ring-diagram calculations with the inclusion of the NNN force V_{3N}^{med} have described well the nuclear matter saturation properties. It would be useful and of interest to check if this approach is also satisfactory for describing closed-shell nuclei whose nucleons are mainly embedded in a similar nuclear medium of densities near ρ_0 , the nuclear matter saturation density. To study this possibility, we have extended the above ring-diagram nuclear matter calculation to the closed shell nucleus ^{16}O , using the same low-energy parameters C_D and C_E (-2.70 and 0.70) determined earlier. Note that these parameters will also be used later in our *sd* and *sdpf* shell-model calculations. Our ring-diagram calculation for ^{16}O is quite similar to the nuclear matter one. The ground-state energy shift for ^{16}O is also given by the all-order sum of the ring diagrams illustrated in Fig. 3, except for the following differences. For nuclear matter, the s.p. states are plane-wave states and each particle line in the figure denotes a plane-wave particle with momentum $k > k_F$ and each hole line with $k < k_F$. For ^{16}O we use harmonic oscillator s.p. wave functions ($\hbar\omega=14$ MeV), and each particle line in the figure denotes a nucleon in the particle shells (*1s0d1p0f*), and each hole line a nucleon in the *0s0p* shells. For nuclear matter, we use momentum model space where all particles have momentum $k < \Lambda$. For ^{16}O , we use an oscillator model space composed of the s.p. orbits of the *0s0p1s0d1p0f* shells. Indeed the ring-diagram calculations for nuclear matter and ^{16}O are quite similar. The ground-state energy shift for ^{16}O is also given by Eq.(12), except that the orbits (*ijkl*) now all refer to shell-model orbits and the summation restriction of (*ijkl* $< \Lambda$) is replaced by that of *ijkl* belonging to the above oscillator model space.

With the same V_{2N} and V_{3N}^{med} interactions used for our nuclear matter calculations, we have carried out ring-diagram calculations for the ground-state energy of ^{16}O . Since V_{3N}^{med} is dependent on the nuclear density ρ , we need to have the value of ρ to carry on the calculation. For nuclear matter, this ρ is well defined, but not so for finite nuclei. A preliminary estimate for the density for ^{16}O can be made by considering it as a uniform sphere [33]; in this way the average density for ^{16}O is estimated as $\sim 0.85\rho_0$. A more realistic estimate for this density should be lower, as physically the nuclear surface is diffused (not sharp). In Table I we present results for the ground-state energy per nucleon of ^{16}O for several densities, $\rho/\rho_0 = 0, 0.5, 0.70$ and 0.75 . As seen, the binding energy calculated with $\rho = 0$ (i.e. no V_{3N}^{med}) is clearly not adequate. The inclusion of V_{3N}^{med} lowers the ground-state energy per nucleon significantly; for example the inclusion of V_{3N}^{med} at $\rho/\rho_0=0.75$ has increased the ring-diagram ground-state energy from -6.97 (only V_{2N}) to -8.01 MeV (with V_{3N}^{med}) per nucleon, in good agreement with experiment. Since we have not included the Coulomb interaction in our calculations, an empirical Coulomb energy of 1.14 MeV per nucleon [33] has been included in the above calculation for the ground-state energy of ^{16}O . It

TABLE I: Ring-diagram calculations of the ground-state energy per nucleon E_0 for ^{16}O . The interaction $(V_{2N} + V_{3N}^{med})$ is used. The potential energy per nucleon given by the 1st-, 2nd- and all-order ring diagrams are denoted respectively by PE-1st, PE-2nd and PE-ring. $E_0 - 1st$ and $E_0 - ring$ are given by the 1st- and all-order ring diagrams respectively. The experimental result is from [32]. All energies are in MeV.

ρ/ρ_0	PE-1st	PE-2nd	PE-ring	$E_0 - 1st$	$E_0 - ring$
0	-19.84	-1.99	-23.02	-3.61	-6.79
0.50	-20.67	-2.28	-23.60	-4.44	-7.37
0.70	-20.78	-2.38	-24.11	-4.55	-7.87
0.75	-20.79	-2.40	-24.25	-4.56	-8.01
$E_o - exp$					-8.00

may be noted that our results for $\rho/\rho_0 = 0.70$ and 0.75 are rather close to each other. We have calculated the potential energy (PE) from the $(V_{2N} + V_{3N}^{med})$ interaction. Results given by the 1st- and 2nd- and all-order ring diagrams, denoted by PE-1st, PE-2nd and PE-ring respectively, are listed in the Table. It may be noted that PE-2nd is much smaller than PE-1st. And the difference between (PE-1st+PE-2nd) and PE-ring is rather small, about 5%. Bogner *et al.* [34] have found that V_{low-k} is suitable for perturbative nuclear matter calculations. The good convergence shown in Table I suggests that this interaction is also suitable for perturbative calculations of finite nuclei.

Having seen that the medium-dependent three-nucleon force V_{3N}^{med} has given desirable results for nuclear matter and closed-shell nucleus ^{16}O , we shall now study its effects on the nuclear effective interactions for the degenerate sd one-shell and the non-degenerate $sdpf$ two-shell model spaces. We use the same methods as described in [25] for the calculation and application of these effective interactions, except for the following difference: In [25] only the two-nucleon interaction V_{2N} was employed. In the present work we include both V_{2N} and V_{3N}^{med} . We first calculate the low-momentum interactions from these interactions, and using them to obtain the \hat{Q} -box diagrams as shown in Figs. 1 and 2. The same V_{2N} and V_{3N}^{med} interactions we used earlier in our calculations for nuclear matter and ^{16}O are employed. The degenerate sd and non-degenerate $sdpf$ effective interactions are obtained from the \hat{Q} -box using respectively the LS iteration method [19, 20] and the EKKO iteration method [21, 25]. The nondegenerate $sdpf$ effective interactions can also be calculated using the KK iteration method [23–25].

We first apply the above effective interactions with V_{3N}^{med} to nuclei ^{18}O and ^{18}F . Since V_{3N}^{med} is density dependent, we need to know the ‘local density’ ρ_v felt by the valence nucleons in these nuclei. It should be small, but its precise value is rather uncertain. In the present work, we shall estimate ρ_v by comparing the density profile of ^{16}O and that for the valence nucleons. In Fig. 6 we

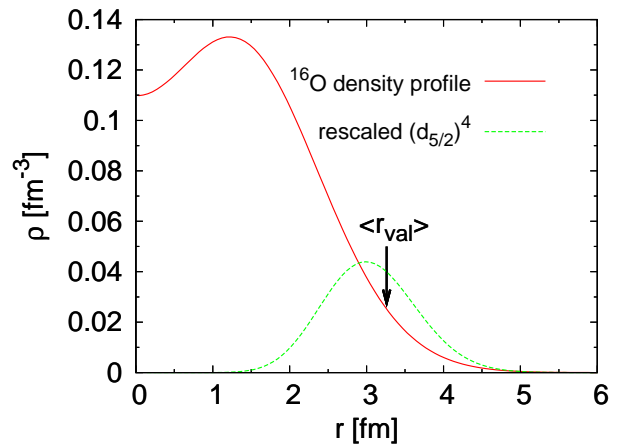


FIG. 6: Density profile of ^{16}O (solid line) and the radial distribution of the fourth power of the $0d$ shell-model wave function (dashed line). See text for other explanations.

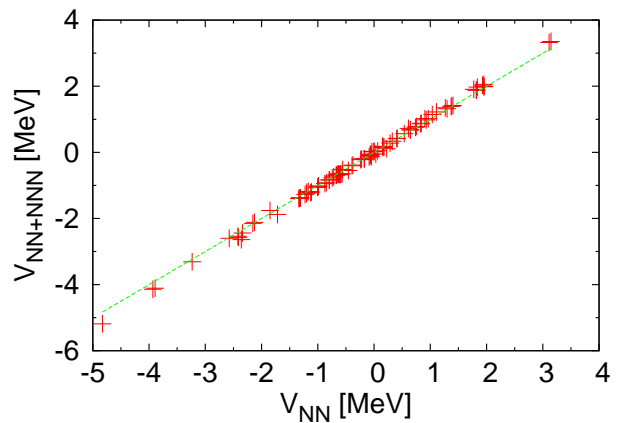


FIG. 7: Comparison of the sd -shell matrix elements of V_{eff} calculated from V_{2N} alone (NN) and from $V_{2N} + V_{3N}$ (NN+NNN).

plot the density profile $\rho_{core}(r)$ of ^{16}O obtained with its wave function assumed to be a closed shell-model s^4p^{12} core. We also plot the distribution $\Phi(r) = \xi\phi(r)^4$ where $\phi(r)$ is the radial harmonic oscillator wave function for $d_{5/2}$, with the scaling parameter $\xi=0.1$. As seen from the plots, the pair of $d_{5/2}$ nucleons reside primarily in the low-density region of ρ_{core} . Depending on the averaging procedure employed, we have estimated ρ_v from $\rho_{core}(r)$ and $\phi(r)$, obtaining values ranging from ~ 0.015 to $\sim 0.030\text{fm}^{-3}$. We have considered another scheme to estimate ρ_v . The rms radius $\langle r_{val} \rangle$ for the shell-model $d_{5/2}$ orbit is indicated by an arrow in the figure. A simple scheme to estimate ρ_v is to let it equal to $\rho_{core}(\langle r_{val} \rangle)$, the value obtained in this way being $\sim 0.025\text{fm}^{-3}$. This value may be reduced if realistic s.p. wave functions are employed. The $d_{3/2}$ orbit is nearly unbound, and its rms radius should be considerably larger than that for $d_{5/2}$. Assuming $\hbar\omega = 10$ MeV for the $d_{3/2}$ orbit, its $\langle r_{val} \rangle$

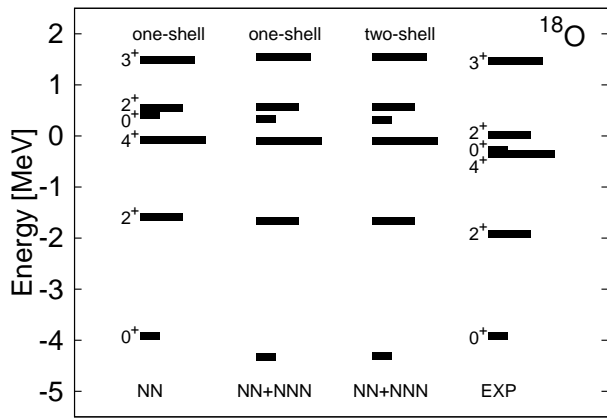


FIG. 8: Energy spectrum of ^{18}O calculated from V_{2N} alone (NN) and from $V_{2N} + V_{3N}$ (NN+NNN). The sd (one-shell) and $sdpf$ (two-shell) model spaces are both employed. The experimental results are from [32].

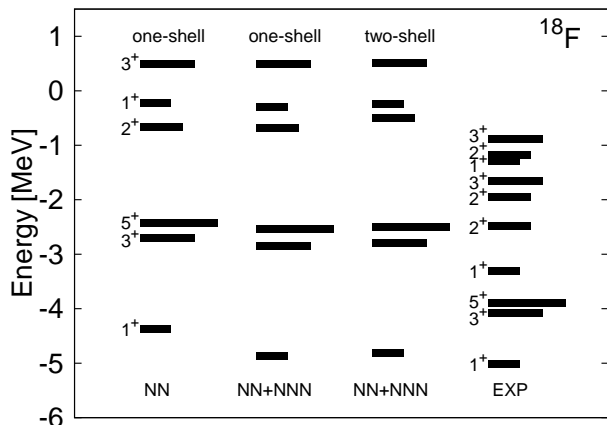


FIG. 9: Same as Fig. 8 except for ^{18}F .

would be $\sim 3.8\text{fm}$ giving $\rho_v \simeq 0.01\text{fm}^{-3}$ for this orbit. We believe that a suitable range for ρ_v is from ~ 0.1 to $\sim 0.2\rho_0$ ($\rho_0 \equiv 0.16\text{fm}^{-3}$). In the present work, we adopt $\rho_v = 0.15\rho_0$, to illustrate the effects of V_{3N}^{med} .

In Fig. 7 the matrix elements of the sd -shell effective interactions calculated from V_{2N} with and without V_{3N}^{med} , denoted respectively as 'NN+NNN' and 'NN', are compared. As seen, the two sets of matrix elements are rather similar to each other, with the magnitudes of those including V_{3N}^{med} being slightly larger. The low-lying spectrum of ^{18}O and ^{18}F calculated with the above interactions are presented in Figs. 8 and 9. The main effect of the 'NNN' force is a small downward shift for the ground states of ^{18}O and ^{18}F , while leaving the other states largely unchanged. This trend is consistent with what we have observed for nuclear matter calculations (see Fig. 4), namely the effect of V_{3N}^{med} is slightly attractive at low densities. With the inclusion of the 'NNN' force, the ground-state energy of ^{18}F is in good agreement with

experiment while that for ^{18}O is slightly overbound. The agreements of the other states with experiments for ^{18}O are better than ^{18}F .

Using the method outlined in section II and [25], we have also calculated the effective interaction for a $sdpf$ two-shell space using V_{2N} with and without the inclusion of V_{3N}^{med} . In Figs. 8 and 9, the spectra of ^{18}O and ^{18}F obtained with the former effective interaction are also presented ('two-shell', 'NN+NNN'). As seen, the 'two-shell' and 'one-shell' results are rather similar to each other. To further study the effects of the three-nucleon force V_{3N}^{med} , we have extended the calculations of Figs. 8 and 9 to nuclei ^{19}O and ^{19}F , with results presented in Figs. 10 and 11. Here, similar to ^{18}O and ^{18}F , the ground-state energies of ^{19}O and ^{19}F obtained with V_{2N} only are both too high compared with experiments (see the 'NN' columns). As shown by the 'NN+NNN' columns, the inclusion of V_{3N}^{med} slightly lowers these energies. The 'one-shell' and 'two-shell' results are rather close to each other for ^{19}O . But they are slightly different for ^{19}F , with the 'NN+NNN' ground-state energy noticeably lower than the 'NN' one.

As shown in Figs. 8-11, although there are qualitative agreements between the calculated and experimental spectra of ^{18}O , ^{18}F , ^{19}O and ^{19}F , there are significant disagreements between them. For example, the orderings of the calculated low-lying states of ^{19}O are in fair agreement with the experimental ones, but their relative spacings are not. As shown by the figures, the effects from V_{3N}^{med} are generally small and attractive, mainly slightly lowering their ground-state energies while having nearly no influence on the relative spacings of the calculated spectrum. It should be useful to further study how to reduce the above disagreements. We have employed a low-order approximation for the \hat{Q} -box, including only 1st- and 2nd-order diagrams. The inclusion of higher-order diagrams may alter our results. As carried out by Holt et al. [35], certain classes of planar diagrams of the \hat{Q} -box can be summed up to all orders using the Kirson-Babu-Brown induced interaction method. We plan to extend our present calculations by including these planar diagrams, and study their effects to the shell-model description of these nuclei. ?

IV. SUMMARY AND CONCLUSION

We have carried out shell-model calculations for nuclei ^{18}O , ^{18}F , ^{19}O , ^{19}F and ^{16}O using effective interactions derived from the chiral two- and three-nucleon potentials. We start from the $N^3\text{LO}$ two-nucleon potential V_{2N} together with an in-medium three-nucleon potential V_{3N}^{med} which is a density-dependent effective interaction derived from the lowest-order chiral three-nucleon force V_{3N} by Holt, Kaiser and Weise [10, 11]. The V_{low-k} low-momentum interactions are then derived from these potentials, and are used in a folded-diagram expansion

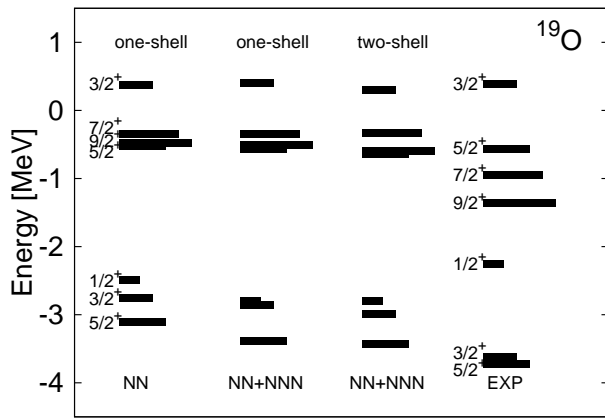


FIG. 10: Same as Fig. 8 except for ^{19}O .

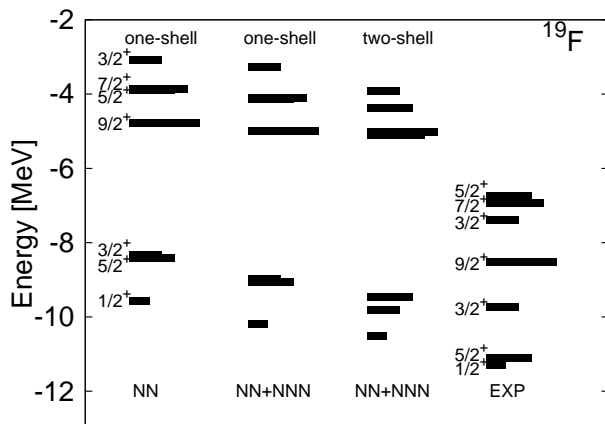


FIG. 11: Same as Fig. 8 except for ^{19}F .

for calculating the V_{eff} interactions for both the degenerate sd and non-degenerate $sdpf$ model spaces. The well-known Lee-Suzuki iteration method [19, 20] is used for the derivation of the sd effective interactions, while the recently developed iteration method of Okamoto *et al.* [21] is employed for the $sdpf$ ones.

We have studied the effects of V_{3N}^{med} , which is an effective two-body interaction depending on the medium density ρ , at various densities near and below the nuclear matter saturation density ρ_0 . We first apply the V_{3N}^{med} interaction to nuclear matter calculations for which the medium density is uniform and well defined. A ring-diagram method for nuclear matter has been employed. The low-energy constants C_D and C_E , of respectively the one-pion and contact terms of the leading-order chiral three-nucleon potential V_{3N} , are not well known. We have chosen these constants by requiring that their use in our nuclear matter calculations with V_{2N} and V_{3N}^{med} , which is derived from V_{3N} , satisfactorily reproduces the saturation properties of nuclear matter. As indicated in Fig. 4, the inclusion of V_{3N}^{med} has largely improved our nuclear matter results comparing with those given by V_{2N}

alone, and the resulting nuclear matter saturation properties are in good agreement with the empirical values.

We then calculate the sd and $sdpf$ effective interactions with the inclusion of the above V_{3N}^{med} , and apply them to nuclei ^{18}O , ^{18}F , ^{19}O and ^{19}F . An ambiguity here is the determination of the local density ρ_v felt by the valence nucleons of these nuclei. This density should be small compared with the saturation density ρ_0 of nuclear matter, but it is difficult to determine its value precisely. We have estimated this value based on the density profile of ^{16}O given by a simple s^4p^{12} shell-model wave function. This is an approximation which should be further investigated and improved upon. In our calculations for these nuclei, we have adopted the estimation of $\rho_v/\rho_0=0.15$. As indicated by Figs. 8-11, the main effect of V_{3N}^{med} is to lower the ground-state energies of these nuclei slightly, making them in better agreements with experiments than the energies given by V_{2N} alone. The effects of V_{3N}^{med} to these nuclei are general small, mainly because their valence nucleons are in a low-density medium.

The above V_{3N}^{med} has also been applied to a shell-model calculation of closed-shell nucleus ^{16}O . The nucleons in closed-shell nuclei are embedded in nuclear medium of much larger density than that for the valence nucleons mentioned above. For them the effect of V_{3N}^{med} is expected to be more important. Indeed this is confirmed by our calculations. As illustrated in Table I, the inclusion of this interaction has been essential for satisfactorily reproducing the empirical binding energy of ^{16}O . It should be useful and of interest to further study this in-medium three-nucleon potential by applying it to closed-shell nuclei and those with a few valence holes.

We are very grateful to L. Coraggio, A. Covello, A. Gargano, N. Itaco, M. Machleidt and R. Okamoto for many helpful discussions. Partial supports from the US Department of Energy under contracts DE-FG02-88ER40388 and the DFG (Deutsche Forschungsgemeinschaft) cluster of excellence: Origin and Structure of the Universe are gratefully acknowledged.

-
- [1] B.A. Brown and B.H. Wildenthal, Ann. Rev. Nucl. Part. Sci. **38**, 29(1988).
 - [2] B.A. Brown, W.A. Richter, Phys. Rev. C **74**, 0343150 (2006).
 - [3] M. Hjorth-Jensen, T. T. S. Kuo, and E. Osnes, Phys. Rep. **261**, 126 (1995), and references therein.
 - [4] L. Coraggio, A. Covello, A. Gargano, N. Itaco and T.T.S. Kuo, Prog. Part. Nucl. Phys., **62** (2009) 135, and references quoted therein.
 - [5] L.W. Siu, J.W. Holt, T.T.S. Kuo and G.E. Brown, Phys. Rev. **C79**, 054004 (2009).
 - [6] H. Dong, T.T.S. Kuo and R. Machleidt, Phys. Rev. **C80**, 065803 (2009).
 - [7] A. Nogga, H. Kamada and W. Glockle, Phys. Rev. Lett. **94**, 944(2000).
 - [8] S.C. Peiper, K. Varga and R. B. Wiringa, Phys. Rev.

- C66**, 044310 (2002).
- [9] P. Navratil, V.G. Gueorguiev, J.P. Vary, W.E. Ormand and A. Nogga, *Phys. Rev. Lett.* **99**, 042501(2007).
- [10] J. W. Holt, N. Kaiser and W. Weise, *Phys. Rev.* **C79**, 054331 (2009).
- [11] J. W. Holt, N. Kaiser and W. Weise, *Phys. Rev.* **C81**, 024002 (2010).
- [12] T. Otsuka, T. Suzuki, J.D. Holt, A. Schwenk and Y. Akaishi, *Phys. Rev. Lett.* **105**, 032501 (2010).
- [13] D. R. Entem, R. Machleidt, and H. Witala, *Phys. Rev. C* **65**, 064005 (2002).
- [14] S. K. Bogner, T. T. S. Kuo and L. Coraggio, *Nucl. Phys.* **A684**, (2001) 432.
- [15] S.K. Bogner, T.T.S. Kuo, L. Coraggio A. Covello, and N. Itaco, *Phys. Rev. C* **65**, 051301(R) (2002).
- [16] S. K. Bogner, T. T. S. Kuo, and A. Schwenk, *Phys. Rep.* **386**, 1 (2003).
- [17] T. T. S. Kuo and E. Osnes, *Lecture Notes in Physics* (Springer-Verlag, New York, 1990), Vol. 364.
- [18] T.T.S. Kuo, S.Y. Lee and K.F. Ratcliff, *Nucl. Phys.* **A176** (1971) 172.
- [19] S.Y. Lee and K. Suzuki, *Phys. Lett.* **91B**, 173 (1980).
- [20] K. Suzuki and S.Y. Lee, *Prog. Theor. Phys.* **64**, 2091 (1980).
- [21] R. Okamoto, K. Suzuki, H. Kumagai and S. Fujii, to be published in 'Proceedings of the 10th International Spring Seminar on Nuclear Physics (May 21-25, Sur Mare Vietri, Italy, ed. by A. Covello)'; [nucl-th] arXiv:1011.1994v1.
- [22] K. Suzuki, R. Okamoto, P.J. Ellis and T.T.S. Kuo, *Nucl. Phys.* **A567** (1994) 576.
- [23] E.M. Krenciglowa and T.T.S. Kuo, *Nucl. Phys.* **A235**, 171 (1974).
- [24] T.T.S. Kuo, F. Krmpotic, K. Suzuki and R. Okamoto, *Nucl. Phys.* **A582**, 205(1995).
- [25] H. Dong, T.T.S. Kuo and J.W. Holt, preprint (May 2011, to be submitted to arXiv and PRC).
- [26] H. Q. Song, S. D. Yang and T.T.S. Kuo, *Nucl. Phys.* **A462**, 491 (1987).
- [27] M. C. M. Rentmeester, R. G. E. Timmermans, and J. J. de Swart, *Phys. Rev. C* **67** (2003) 044001.
- [28] E. Epelbaum, *Prog. Part. Nucl. Phys.* **57**, 654(2006).
- [29] R. Machleidt, *Phys. Rev. C* **63**, 024001 (2001).
- [30] R. B. Wiringa, V. G. J. Stoks, and R. Schiavilla, *Phys. Rev. C* **51**, 38 (1995).
- [31] V. G. J. Stoks, R. A. M. Klomp, C. P. F. Terheggen, and J. J. de Swart, *Phys. Rev. C* **49**, 2950 (1994).
- [32] <http://www.nndc.bnl.gov/chart/>.
- [33] P. Ring and P. Schuck, *The Nuclear Many-Body Problem* (Springer-Verlag, New York, 1980).
- [34] S. K. Bogner, A. Schwenk, R. J. Furnstahl and A. Nogga, *Nucl. Phys.* **A763** (2005) 59.
- [35] J. D. Holt, J. W. Holt, T. T. S. Kuo, G. E. Brown and S. K. Bogner, *Phys. Rev.* **72**, 041304R (2005).